A 3D Ultrasound algorithm with alignment and nonlinearity compensation

J. Sanches and J. S. Marques
Instituto Superior Técnico / Instituto de Sistemas e Robótica
Av. Rovisco Pais, 1049-001 Lisboa
Portugal
jmrs@alfa.ist.utl.pt

Keywords: image reconstruction, alignment, log-compression, medical imaging, multiplicative noise

Abstract: This paper describes a system to reconstruct a 3D region of the human body from a set of ultrasound images. Several issues make this problem difficult: non uniform sampling of the 3D region, the presence of multiplicative noise (specke), the non linear compression of the ultrasound images performed during the acquisition process and image misalignment. A reconstruction algorithm is proposed which takes all these issues into account in a Bayesian framework. An interpolation model is adopted to define the acoustic reflectivity of the human tissues in the region of interest. The volume coefficients as well as the alignment and compression parameters are estimated by the minimization of a single objective function in three consecutive steps, performed in each iteration of the reconstruction algorithm. Experimental results are presented to assess the performance of the algorithm.

1 Introduction

Ultrasound systems are widely used in medical diagnosis. Most of them operate in B-scan mode allowing the visualization of cross sections of the human body, in real time (Quistgaard, 1997). B-scan provides valuable anatomical cues but has several limitations, namely, it does not allow the visualization of the organs surface, accurate volume measurement or the visualization of arbitrary cross sections of the human body. 3D ultrasound has been proposed to overcome these difficulties.

3D ultrasound aims to visualize the human body in a given region of interest from a set of ultrasound images (Rohling et al.,1996). The Fig.1 shows the architecture of a 3D ultrasound system, including a data acquisition block which produces sequences of ultrasound images as well the position and orientation of each observed image.

Two approaches have been adopted in the literature to achieve this goal (Nelson et al., 1999): volume reconstruction, e.g. see (Carr, 1996; Sanches et al., 2000) and surface estimation, e.g. see (Raya et al., 1990; Tagare, 1999; Treece et al., 1999). In both cases, the main difficulties concern: i) non uniform sampling (some regions of the human body are not observed), ii) multiplicative noise; iii) unknown pre processing and iv) misalignment. Each of these difficulties is briefly described:

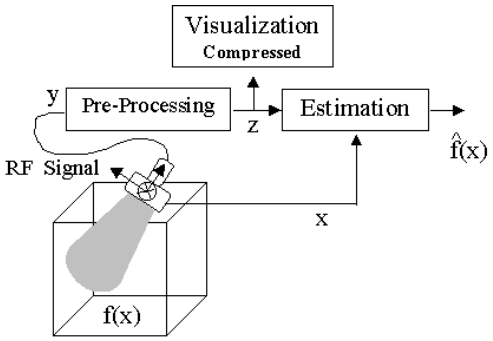

Figure 1: Acquisition system.

a) Speckle noise

The RF signal produced by the ultrasound probe is corrupted by multiplicative noise similar to the one observed in LASER (Abbot et al.,1979) or SAAR (Dias et al., 1998) measurements. This noise is produced by the interaction of coherent radiation with a large number of scatters and it has Rayleigh distribution (Burckhardt, 1978).

When the number of scatters is low or some of them are stronger than the others, the Rayleigh distribution

is no longer valid (Narayanan et al., 1994) and other distributions should be used instead (e.g. the K distribution (Jakeman et al., 1976)). This situation occurs at the organ surfaces where specular reflections lead to pixel intensities which can not be described by a Rayleigh model. The speckle noise present in ultrasound images must be explicitly considered in the design of a reconstruction algorithm.

b) Nonlinear Compression

The dynamic range of the RF signal (typically 60dB) is higher than the dynamic range of the monitor used to display the images (typically 25dB) (Dutt, 1996). The ultrasound equipment compresses the RF signal in a preprocessing block, using a logarithmic function (Lopas et al., 1989). Furthermore, the user may change the compression parameters to improve visualization. Therefore, the pre-processing parameters are not known in advance. Unfortunately the processing changes the probability distribution of the ultrasound images which become no longer Rayleigh. In order to use the Rayleigh model we have to estimate the compression parameters used in each experiment to expand the observed images.

c) Misalignment

There are two main reasons for image misalignment.

The ultrasound probe must be kept under pressure during the acquisition process in order to obtain good acoustic coupling. This procedure modifies the organ shapes and positions leading to significant geometric errors that degrade the final reconstruction.

The position and orientation of each image are measured by an electromagnetic locator (Fasttrack, 1993; Carr, 1996). This information allows to compute the 3D position of each image pixel used in the reconstruction process. However, the pose parameters are corrupted by measurements errors which must be compensated in the reconstruction process. This paper describes a system for 3D reconstruction which takes these difficulties into account in a Bayesian framework. The proposed algorithm consists of three steps which are iteratively performed as shown in Fig.2.

The paper is organized as follows. Section 2 formulates the problem and section 3 presents the models used for estimation proposes. Section 4 addresses optimization issues. Section 5 presents experimental results and Section 6 concludes the paper.

2 Problem formulation

Let U be a set of parameters defining the acoustic impedance in the region to be reconstructed . Let D be a set of alignment parameters associated with each cross section and θ the parameters defining the compression function used in the pre-processing step by the ultrasound equipment. The exact meaning of these parameters is clarified in the next sections.

The goal of the reconstruction algorithm is to simultaneously estimate these parameters in a Bayesian framework using a MAP criterion. This problem can be formulated as follows

$$(\hat{U}, \hat{D}, \hat{\theta}) = arg \max_{U,D,\theta} J(U, D, \theta, V) \quad (1)$$

where V is the observed data, i.e., the image sequence and the positions and orientations of the ultrasound probe and $J(U, D, \theta, V)$ is an objective function to be maximized.

J is the logarithmic of the joint probability density function of the data and the unknown variables,

$$J(U, D, \theta, V) = \log\left[(p(V|U, D, \theta)p(U)p(D)p(\theta))\right] \quad (2)$$

In this paper, a uniform prior is considered for $p(\theta)$.

The optimization procedure is decomposed in three steps, as shown in Fig.2: 1)volume reconstruction, 2)non linearity estimation and 3)alignment. The three steps are performed in each iteration until convergence is achieved. In each step the objective function (2) is maximized with respect to each set of parameters leading to the following optimization problem

1st step - Volume reconstruction

$$\hat{U} = arg \max_{U} J(U, \hat{D}, \hat{\theta}, V) \quad (3)$$

2nd step - Alignment

$$\hat{D} = arg \max_{D} J(\hat{U}, D, \hat{\theta}, V) \quad (4)$$

3rd step - Non linearity

$$\hat{\theta} = arg \max_{\theta} J(\hat{U}, \hat{D}, \theta, V) \quad (5)$$

3 Models

This section describes in detail the models used for 3D reconstruction of the human organs in the region of interest.

3.1 Volume representation

The system developed in this paper aims to reconstruct the tissue reflectivity, f, in a given region of interest Ω.

It is assumed that f belongs to a class of admissible functions defined in a spatial domain, $\Omega \subset R^3$, i.e., $f : \Omega \rightarrow R$. Furthermore, it is assumed that the set of admissible functions is a finite dimension vector space $\mathbf{F}$ with known basis functions, ($b_i : \Omega \rightarrow R$). Each function $f \in \mathbf{F}$ can be expressed as a linear combination of the basis functions,

$$f(x) = \Phi(x)^T U \quad (6)$$

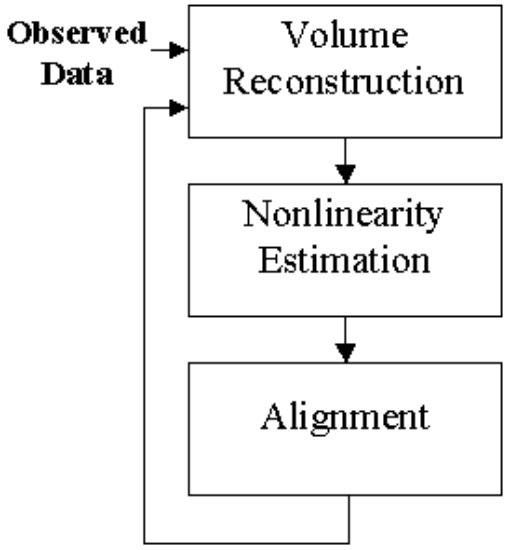

Figure 2: Three step estimation algorithm: a)Volume estimation, b)Nonlinearity function estimation and c)Alignment.

where $\Phi(x) = [\phi_1(x), \phi_2(x), ..., \phi_N(x)]^T$ is a vector of basis functions and $U = [u_1, u_2, ..., u_N]^T$ is a Nx1 vector of coefficients. The estimation of f resorts to the estimation of the unknown coefficients U. It is

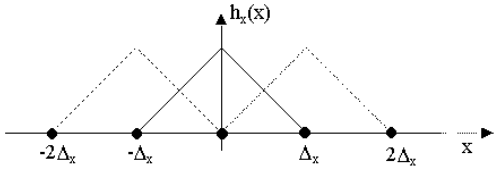

Figure 3: 1D basis function.

assumed that each $\phi_i(x)$ is a local function obtained by shifting a known function $h : R^3 \rightarrow R$, i.e.,

$$\phi_i(x) = h(x - \mu_i) \tag{7}$$

where $\mu_i \in R^3$ is the i-th node of a cubic grid (see Fig. 4) defined in Ω. In this paper it is assumed that h is a tri-linear interpolation function defined by:

$$h(x) = \begin{cases} \prod_{i=1}^{3}(1 - \frac{|x^i|}{\Delta}) & x \in \delta, \\ 0 & \text{otherwise.} \end{cases} \tag{8}$$

where x^i is the i-th coordinate of x, Δ is the grid step and $\delta = [-\Delta, \Delta]^3$(see Fig.3). The grid defines a partition of Ω into cubic voxels. It can be concluded from (7,8) that each basis function ϕ_i has a finite support consisting of 8 voxels and each 3D point belongs to 8 support regions. Therefore to compute $f(x_0)$ defined

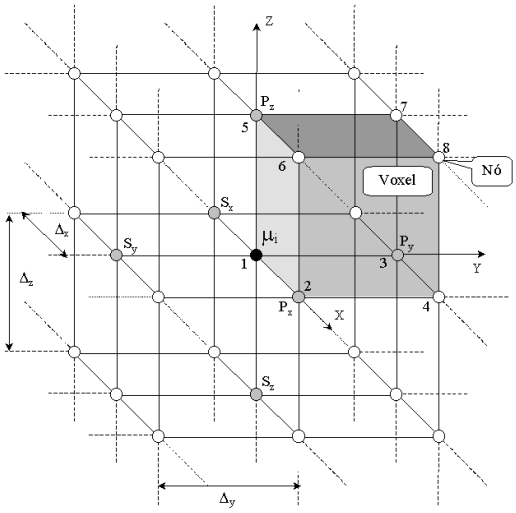

Figure 4: Cubic grid.

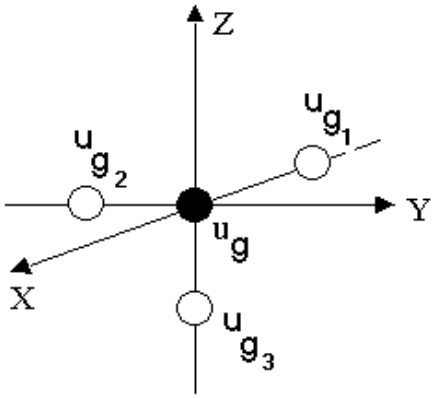

Figure 5: Neighborhood system .

in (6) only 8 coefficients are needed since all the other basis functions are zero at $x = x_0$. A Gibbs prior is adopted for the volume coefficients (Geman, 1984))

$$p(U) = \frac{1}{Z}e^{-\psi \sum_g P(u_g)} = \frac{1}{Z}e^{-\psi \sum_g \sum_i (u_g - u_{gi})^2} \tag{9}$$

where u_{gi} are the neighbors of u_g(see Fig.5) and Z is a normalization factor (see (Sanches et al., 2000) for details). The parameter ψ controls the strength of the links among the neighbors allowing the control of smoothness of the final reconstruction.

3.2 Data Model

The data used to estimate f consists of a sequence of ultrasound images complemented with the trajectory (position and orientation) of the ultrasound sensor during the medical exam. This information al-

lows to compute a set of data points, $V = \{v_i\}$, containing geometric and intensity information i.e., $v_i = (z_i, x_i)$, where z_i is the intensity of the ith pixel and $x_i \in R^3$ its position.

It is assumed that the RF intensities are a set of i.i.d. (independent and identically distributed) random variables with Rayleigh distribution (Burckhardt, 1978; Abbot et al.,1979 ; Wells et al. (1981)). Statistical independence of all elements of Z is considered because the PSF (point spread function) of the image acquisition system is assumed to be smaller than the inter-pixel distance (Dias et al., 1998). The density function associated with y_i is given by

$$p(y_i) = \frac{y_i}{f(T_p(x_i))} e^{-\frac{y_i^2}{2f(T_p(x_i))}} \quad (10)$$

where y_i denotes the RF intensity of i-th pixel of the uncompressed image and $f(T_p(x_i))$ represents the reflectivity associated to the position $T_p(x_i)$. T_p is an alignment function which corrects the position of the pixels of the pth cross-section.

However, y is not available. The observed is the output of the pre processing block, z(see Fig. 1).

In this paper a log-compression law is considered for modeling the pre-processing block. Therefore

$$z_i = g(y_i) = \xi \log(y_i + 1) + \beta \quad (11)$$

where $\theta = (\xi, \beta)$ are unknown parameters to be estimated. Therefore the distribution of z is given by

$$p(z_i) = \left|\frac{dy}{dz}\right| p(y_i) \quad (12)$$

where $p(y)$ is the density function of the non-compressed ultrasound image and dy/dz is the derivative of the inverse compression function. Using (10,12) leads to

$$p(V|U, D, \theta) = \prod_i \left(\frac{w_i(w_i+1)}{\xi f(T_p(x_i))} e^{-\frac{w_i^2}{2f(T_p(x_i))}}\right) \quad (13)$$

where

$$w_i = e^{\frac{z_i - \beta}{\xi}} - 1 \quad (14)$$

3.3 Geometric Errors

In the previous section the position of each pixel is obtained by applying a transformation $T_p(x)$ to the position provided by the spatial locator. This transformation is defined as

$$\hat{x}_i^p = T_p(x_i^p) = x_i^p + d^p \quad (15)$$

where d^p is a displacement vector to be estimated,

$$d^p = d_1^p u_1^p + d_2^p u_2^p \quad (16)$$

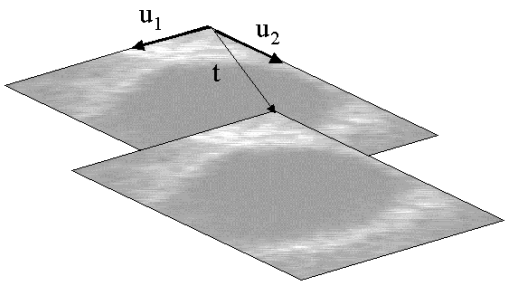

Figure 6: Displacement vector.

where (u_1^p, u_2^p) are two orthogonal vectors, parallel to the inspection plane with length equal to pixel size; $(d_1, d_2)^p$ are coefficients associated to each cross-section defining the length and direction of the displacement vector (see Fig.6). The displacement error d^p is assumed to be the same for all pixels of the p-th cross section.

This model assumes that the displacement vectors belong to the planes associated with the cross-sections. In fact, the most important source of geometric errors is the pressure of the ultrasound probe against the body. It is expected that this compression makes the tissues move along the main axis of the cross section plane.

It is also assumed that the coefficients d_r^p with $r = 1, 2$ are i.i.d. random variable with normal distribution $p(d_r^p) = N(0, \sigma_d^2)$. Therefore,

$$p(D) = \prod_p \frac{1}{2\pi\sigma_d^2} e^{-\frac{\|d^p\|^2}{2\sigma_d^2}} \quad (17)$$

4 Optimization

The objective function to be maximized can now be obtained by replacing (9), (13), (17) in (2), discarding the additive constants

$$\begin{aligned} J(U, D, (\xi, \beta), V) = \\ \sum_i \left[\log\left(\frac{w_i(w_i+1)}{f(x_i)\xi}\right) - \frac{w_i^2}{2f(x_i)}\right] \\ -\frac{1}{2\sigma_d^2} \sum_p \left[(d_1^p)^2 + (d_2^p)^2\right] \\ -\psi \sum_g \sum_i (u_g - u_{gi})^2 \end{aligned} \quad (18)$$

Each step of the algorithm (18) corresponds to the maximization of J with respect to a set of parameters. The sequence of these three maximization processes are irrelevant if the initial estimates of each set

is in the vicinity of the final solution. Each of these optimization problems is addressed below. The initialization procedure will be treated in section 4.4.

4.1 Volume estimation

The optimization of (18) with respect to U is a difficult problem since the number of parameters to estimate is very large (typically millions of coefficients). Furthermore, (18) is a non convex and nonlinear function (Li, 1998), for which there is no closed form solution. Therefore, numerical methods must be considered (Conte et al., 1981).

To solve (3) the ICM algorithm proposed by Besag (Besag, 1986) is used in this paper. The multivariate optimization problem is converted into a sequence of 1D optimization tasks. In each iteration, the objective function is considered as a 1D function depending on a single parameter, keeping all the others constant. During the iterative process all the parameters are sequentially updated, until convergence is achieved.

To maximize (18) with respect to one generic volume coefficient, u_p, the following stationary condition must be met

$$\frac{\partial}{\partial u_p} J(U, D, \theta, V) = 0 \tag{19}$$

Using the fixed point method (**?**) one obtains

$$^{n+1}\hat{u}_p = \frac{1}{4\psi N_v} \sum_i \frac{w_i^2 - 2f(x_i)}{f^2(x_i)} \phi_p(x_i) + \bar{u}_p \tag{20}$$

where

$$w_i = e^{\frac{z_i - \beta}{\xi}} - 1 \tag{21}$$

and

$$\bar{u}_p = \frac{1}{N_v} \sum_{u_g \in \delta_p} u_g \tag{22}$$

N_v is the number of control points inside the neighborhood δ_p of the p-th grid node p($N_v = 6$).

4.2 Alignment

A displacement vector must be estimated for each ultrasound image. Only the pixels of the pth image are used to estimate d^p.

Equation (4) is solved by finding a stationary point of (18) with respect to the displacement vector, d^p, i.e.

$$\nabla_{d^p} J(U, D, \theta, V) = 0 \tag{23}$$

where ∇_{d^p} is the gradient of J with respect to the vector d^p. This equation is solved for each cross-section by using a multidimensional version of the Newton-Rapson algorithm (Bakhvalov, 1976)

$$^{n+1}d^p =^n d^p - D_{upd}^{d^p} \tag{24}$$

where $D_{upd}^{d^p}$ is the updating term

$$D_{upd}^{d^p} = \nabla J_{d^p}(U, D, \theta, V) H_{d^p}(U, D, \theta, V)^{-1} \tag{25}$$

where $H_{d^p}(U, D, \theta, V)$ is the Hessian matrix of J. The computation of $\nabla J_{d^p}(U, D, \theta, V)$ and $H_{d^p}(U, D, \theta, V)$ leads to:

$$^{n+1}\hat{d}_1^p =^n \hat{d}_1^p (1 - \frac{J_2 J_{12} - J_1 J_{22}}{J_{11} J_{22} - J_{12}^2}) \tag{26}$$

$$^{n+1}\hat{d}_2^p =^n \hat{d}_2^p (1 - \frac{J_1 J_{12} - J_2 J_{11}}{J_{11} J_{22} - J_{12}^2}) \tag{27}$$

where $J_1, J_2, J_{12}, J_{11}, J_{22}$ denote partial derivatives of J with respect to d_1, d_2 given by

$$\begin{aligned}
J_1 &= \tfrac{1}{2} \textstyle\sum_i (a_i \frac{\partial f(T^p(x_i^p))}{\partial d_1^p}) - \frac{d_1^p}{\sigma_d^2} \\
J_2 &= \tfrac{1}{2} \textstyle\sum_i (a_i \frac{\partial f(T^p(x_i^p))}{\partial d_2^p}) - \frac{d_2^p}{\sigma_d^2} \\
J_{11} &= -\textstyle\sum_i (b_i (\frac{\partial f(T^p(x_i^p))}{\partial d_1^p})^2) - \frac{1}{\sigma_d^2} \\
J_{22} &= -\textstyle\sum_i (b_i (\frac{\partial f(T^p(x_i^p))}{\partial d_2^p})^2) - \frac{1}{\sigma_d^2} \\
J_{12} &= -\textstyle\sum_i (b_i \frac{\partial f(T^p(x_i^p))}{\partial d_1^p} \frac{\partial f(y_i^p)}{\partial d_2^p})
\end{aligned} \tag{28}$$

In these expressions

$$\begin{aligned}
a_i &= \tfrac{(z_i^p)^2 - 2f(T^p(x_i^p))}{f(T^p(x_i^p))^2} \\
b_i &= \tfrac{(z_i^p)^2 - f(T^p(x_i^p))}{f(T^p(x_i^p))^3}
\end{aligned} \tag{29}$$

The sums in (28), (29) are computed for all the pixels of the p-th image, leading to

$$\frac{\partial f(x)}{\partial d_\tau} = \frac{\partial f(x)}{\partial x} \frac{\partial x}{\partial d_\tau} = \nabla f(x).u_\tau \tag{30}$$

where $\nabla f(x)$ is the gradient of $f(x)$ computed at x and $\nabla f(x).u_\tau$ is the derivative of $f(x)$ along the u_τ direction.

4.3 Compression estimation

To estimate the compression parameters a similar approach is followed based on the solution of the stationary condition

$$\nabla_\theta J(U, D, \theta, V) = 0 \tag{31}$$

As before, a two-dimensional version of the Newton-Rapson method is used to solve 31.

$$^{n+1}\hat{\theta} =^n \hat{\theta} - D_{upd}^{\theta} \tag{32}$$

where D^{θ}_{upd} is the updating term

$$D^{\theta}_{upd} = \nabla_{\theta} J(U, D, \theta, V) H_{\theta}(U, D, \theta, V)^{-1} \quad (33)$$

where $\nabla_{\theta} J(U, D, \theta, V)$ is the gradient vector and H_{θ} is the Hessian matrix with respect to θ. Equation (33) can be rewritten as follows

$$^{n+1}\hat{\xi} =^{n} \hat{\xi}(1 - \frac{J_{\beta} J_{\xi\beta} - J_{\xi} J_{\beta\beta}}{J_{\xi\xi} J_{\beta\beta} - J^2_{\xi\beta}}) \quad (34)$$

$$^{n+1}\hat{\beta} =^{n} \hat{\beta}(1 - \frac{J_{\xi} J_{\xi\beta} - J_{\beta} J_{\xi\xi}}{J_{\xi\xi} J_{\beta\beta} - J^2_{\xi\beta}}) \quad (35)$$

where

$$\begin{array}{l} J_{\xi} = \sum_i A_i \log(w_i + 1) - 1 \\ J_{\xi\xi} = \sum_i 2A_i \log(w_i + 1) + B_i \log^2(w_i + 1) - 1 \\ J_{\beta} = \sum_i A_i \\ J_{\beta\beta} = \sum_i B_i \\ J_{\xi\beta} = \sum_i A_i + B_i \log(w_i + 1) \\ A_i = \frac{w_i^3 + w_i^2 - 2f(T^p(x_i^p))w_i - f(T^p(x_i^p))}{f(T^p(x_i^p))w_i} \\ B_i = \frac{2w_i^3 + w_i^2 + f(T^p(x_i^p))}{f(T^p(x_i^p))w_i^2}(w_i + 1) \end{array} \quad (36)$$

4.4 Initializations

The initialization of the unknown variables is a key step in achieving good reconstruction results. If the initial parameters are far from the true values the optimization algorithm may converge to a local maximum corresponding to a wrong reconstruction of the volume.

In this paper, the displacement parameters are initialized to zero, $(d_i^p = 0)$, since we have assumed that the displacement vectors have.

The initialization of u_p and θ is obtained using the mean and variance of the observed data. However, it is not possible to find closed form expressions for these statistics for the model used in this paper (see (11)). To overcome this difficulty a slightly different model is considered for the compression law

$$z = \xi \log(y) + \beta \quad (37)$$

Assuming that y is a random variable with Rayleigh distribution, $p(z)$ becomes a Fisher-Tippet distribution also known as double exponential distribution (Abramowitz et al., 1972; Dutt, 1996)

$$p(z_i/U) = \frac{w_i^2}{\xi f(x_i)} e^{-\frac{w_i^2}{2f(x_i)}} \quad (38)$$

where $w_i = e^{\frac{z_i - \beta}{\alpha}}$

As it can be verified, this distribution is similar to (13) for the range of values used in ultrasound images $(0 < z_i < 255)$. This suggests the approximation of (13) by (38). The mean and standard deviation of the Fisher-Tippet distribution are given by(Abramowitz et al., 1972)

$$\bar{z} = \xi(\log(2f) - \gamma)/2 + \beta \quad (39)$$

$$\sigma_z = \pi\xi/\sqrt{24} \quad (40)$$

where $\gamma = 0.5772...$ is the Euler-Mascheroni constant.

Based on the above expressions, initial values for the ξ, u parameters can be computed as follows

$$\hat{\xi}_0 = \sqrt{\frac{24}{\pi^2}\sigma_z^2} \quad (41)$$

and

$$\hat{u}_p^0 = 0.5e^{\frac{2\pi(\bar{z} - \min z)}{\sqrt{24\sigma_z^2}} + \gamma} \quad (42)$$

The β parameter will be initialized by

$$\hat{\beta}_0 = \min(z) \quad (43)$$

It was experimentally found that this initialization usually provides good estimates for β. In fact, this is an expected result since $\min(z) = \min(\log(y + 1) + \beta) = log(\min(y) + 1) + \beta = \log(0 + 1) + \beta = \beta$.

5 Experimental Results

The proposed algorithm was tested with synthetic and real data. Only examples with real data will be shown in this paper to keep the paper within the allowed length. The images and 3D measurements used in this work were provided by R. Prager and A. Gee from the University of Cambridge.

Three types of testes are shown to illustrate the performance of the reconstruction algorithm (see Fig.2): results obtained with the basic reconstruction method, with nonlinearity compensation and with alignment.

5.1 Volume Reconstruction

Fig.7 shows the reconstruction results obtained for a sequence of 62 images with 176×176 pixel of a gall bladder (simple sweep[1]) using the method described in section 4.1 without nonlinearity compensation or geometric alignment.

Fig.7.a) shows two ultrasound images of the gall bladder, Fig.7.b) shows the corresponding cross-sections of the reconstructed volume and Fig.7.c) shows two cross sections of the reconstructed volume associated to planes which can not be observed in a medical exam due the geometry of the human body. Fig.7.d) shows the representation of the organ surface obtained by ray-casting. Fig.8 shows the results ob-

[1]The sequence was obtained by sweeping the ultrasound probe in the same direction.

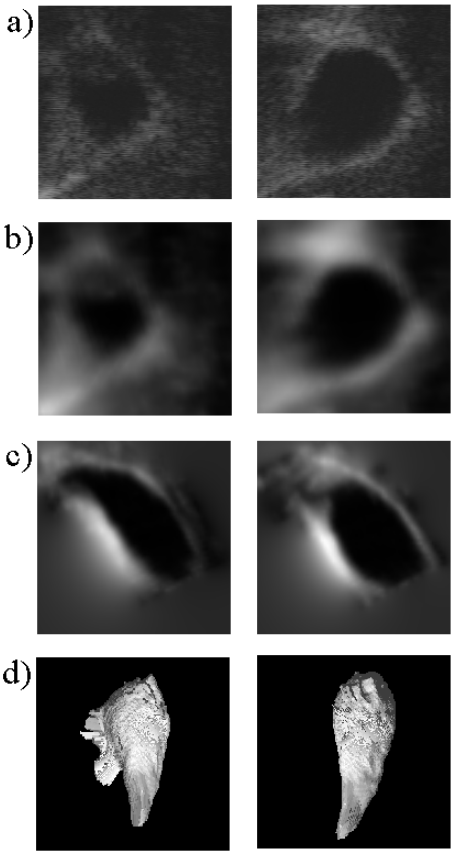

Figure 7: Gall bladder reconstruction. a)Ultrasound images, b)Cross sections extracted from the estimated volume, c)New cross-sections not visible during the inspection process and d)Surface extracted from the estimated volume.

tained with a longer sequence corresponding to two sweeps (94 images) of the ultrasound probe in opposite directions. The misalignment of the images obtained in each sweep produces undesirable artifacts in the reconstruction results as shown in the figure.

5.2 Alignment

The ultrasound images are geometrically distorted. The probe pressure against the tissues distorts the geometry of the human organs. This effect is specially visible in the case of multiple sweeps since the same cross sections are observed several times in different pressure conditions. Misalignment errors such as the ones shown in Fig.8 degrade the reconstruction results.

Fig.9 shows the reconstruction results obtained without and with alignment for a sequence of images obtained by sweeping the ultrasound probe in two opposite directions.

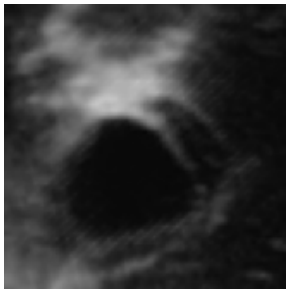

Figure 8: Misalignment effect visible in the reconstructed volume.

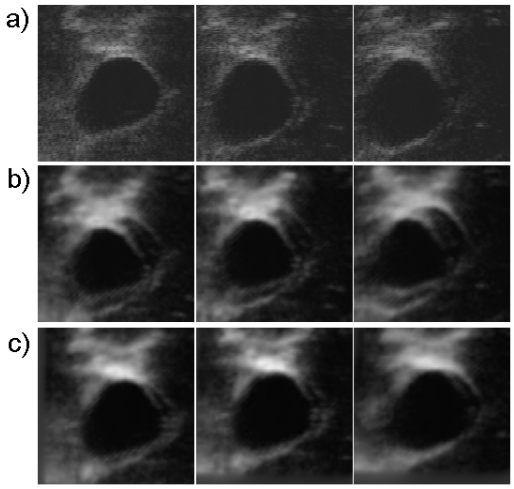

Figure 9: Reconstruction without and with alignment. a)Ultrasound images, b)Correspondent cross sections extracted from the estimated volume without alignment compensation and c)Cross sections extracted from the reconstructed volume using the alignment compensation.

Fig.9.a) shows the original ultrasound images. Fig.9.b) shows the reconstruction results for the corresponding inspection planes, displaying multiple boundary effects. Fig.9.c) shows the results obtained with alignment block. Significant improvements are observed since the presence of multiple shadows for a simple boundary is eliminated.

5.3 Nonlinearity Compensation

The use of the nonlinearity compensation allows to improve the reconstruction results by enhancing anatomic details which are blurred by the basic reconstruction method.

Fig.10 shows the reconstruction results obtained without and with compensation. Fig.10.a) shows the original images and the intensity profiles obtained

without nonlinearity compensation. The organ surface appears somewhat blurred in this image.

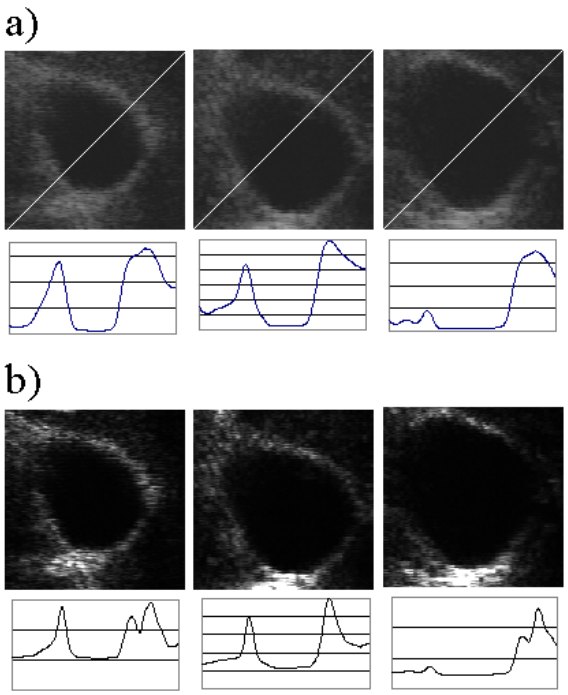

Figure 10: Reconstruction results of a gall bladder. a) Ultrasound images and the corresponding profiles extracted from the estimated volume without nonlinearity compensation. b) Decompressed ultrasound images using the estimated function and the corresponding profiles extracted from the estimated volume using the nonlinearity estimation.

Fig.10 shows the decompressed images obtained using the estimates provided by the nonlinearity estimation algorithm and the corresponding intensity profiles of the reconstruction results obtained with the decompressed images. An improvement is clearly observed, specially in the non stationary regions.

6 Conclusions

3D ultrasound aims to visualize the human body in a given region of interest from a set of ultrasound images. Two approaches have been adopted in the literature to achieve this goal: volume reconstruction and surface detection. In both cases the main difficulties concern non uniform sampling (some regions of the human body are not observed), low signal to noise, nonlinearity compensation, ratio and image misalignment. Instead of relying on ad hoc techniques for dealing with each of these difficulties, this paper proposes a reconstruction algorithm based on the minimization of a single objective function. This function is derived from probabilistic models of the data acquisition process which account for the presence of multiplicative noise with Rayleigh distribution, non linear pre-processing of the ultrasound data with unknown compression function, geometric distortions of the human organs during the medical exam due to the pressure of the ultrasound probe against the body, measurement errors of the probe position and orientation. An optimization algorithm is described based on three steps: Rayleigh reconstruction, non-linearity estimation and image alignment. These steps are iteratively performed until convergence is achieved. Experimental results with real data are present to assess the performance of the algorithm. It is shown that each of the three steps performs an important role to improve the reconstruction results.

Acknowledgments

The ultrasound data used in this work was kindly provided by R.Prager and A.Gee from the University of Cambridge.

This work was partially supported by the FCT (Heart 3D project).

REFERENCES

J. Abbot and F. Thurstone, Acoustic Speckle: Theory and Experimental Analysis, Ultrasound Imaging vol.1, pp.303-324, 1979.

M. Abramowitz and I. A. Stegun, Handbook of Mathematical Functions with Formulas, Graphs, and Mathematical Tables, 9th ed. New York:Dover, 1972.

N. Bakhvalov, Mthodes Numriques, Editions Mir, Moscou 1976.

J. Besag, On the Statistical Analysis of Dirty Pictures, J. R. Statist. Soc. B, vol.48, no. 3, pp. 259-302, 1986.

C. Burckhardt, Speckle in Ultrasound B-Mode Scans, IEEE Trans. on Sonics and Ultrsonics, vol. SU-25, no.1, pp.1-6, January 1978.

J. Carr, Surface Reconstruction in 3D Medical Imaging, Ph D. Thesis, University of Canterbury, 1996.

S. D. Conte, C. Boor,Elementary Numerical Analysis, An Algorithmic Approach, McGraw-Hill, 1981.

J. Dias, T.Silva and J. Leitão, Adaptive Restoration of Speckled SAR Images Using a Compound Random Markov Field, Procedings ICIP98 Chicago, vol.II, pp.79-83, October 1998

V. Dutt, Adaptative Speckle Reduction Filter for Log-Compressed B-Scan Images, IEEE Trans. Medi-

cal Imaging. vol.15, no.6,pp.802-813 December 1996.

3SPACE, Fasttrak, Users's Manual, Revision F, Polhemus, November 1993.

S. Geman and D. Geman, Stochastic Relaxation, Gibbs Distributions, and the Bayesian Restoration of Images, IEEE Trans on Pattern Analysis and Machine Intelligence, vol.PAMI-6, no.6, pp.721-741, November 1984.

E. Jakeman and P. N. Pusey, A Model for Non-Rayleigh See Echo, IEEE Transactions on Antennas and Propagation, Vol. AP-24, no.6, pp.806-814, November 1976.

S.Z.Li, Close-Form Solution and Parameter Selection for Convex Minimization-Based Edge-Preserving Smoothing, IEEE Trans. on PAMI, vol. PAMI-20, no.9, pp.916-932, September 1998.

T.Loupas, W.N.McDicken, P.L.Allan, An Adaptative Weighted Median Filter for Speckle Supression in Medical Ultrasonic Images, IEEE Trans. on Circuits and Systems, vol.36, no.1, pp.129-135, January 1989.

V. M. Narayanan, P. M. Shankar, J. M. Reid, Non-Rayleigh Statistics of Ultrasonic Backscattered Signals, IEEE Trans. on Ultras., Ferr. and Freq. Control, vol.41, no.6, November 1994.

T. Nelson, D. Downey, D. Pretorius, A. Fenster, Three-Dimensional Ultrasound, Lippincott, 1999.

W.H.Press, W.T.Vetterling, S.A.Teukolsky and B.P.Flanner, Numerical Recipes in C, Cambridge University Press,1994.

J. Quistgaard, Signal Acquisition and Processing in Medical Diagnostics Ultrasound, IEEE Signal Processing Magazine, vol.14, no.1, pp 67-74, January 1997.

S.P. Raya, J.K. Udupa, Shape-Based Interpolation of Multidimensional Objects, IEEE Trans. on Medical Imaging, vol.9, no.1, pp3-42, March 1990.

R.N.Rohling and A.H.Gee, Issues in 3-D Free-Hand Medical Ultrasound Imaging, CUED/F-INFENG/TR 246, January 1996

J. Sanches, J. Marques, A Rayleigh reconstruction/interpolation algorithm for 3D ultrasound, Pattern Recognition Letters, 21, pp.917-926, 2000.

H.D. Tagare, Shape-Based Nonrigid Correspondence with Application to Heart Motion Analysis, IEEE Trans. on Medical Imaging, vol.18, no.7, pp.570-579, July 1999.

G.M.Treece, R.W.Preager, A.H.Gee and L. Berman, Fast surface and volume estimation from non-parallel cross-sections, for frehand 3-D ultrasound, Medical Image Analysis, vol.3, no.2, pp.141-173, 1999.

P.N.T. Wells, M.Halliwell, Speckle in ultrasonic imaging, Ultrasonics, September 1981.